DEFORMATION MECHANISMS OF METALS UNDER COMPLEX NONPROPORTIONAL CYCLIC LOADINGS

S. H. Doong and D. F. Socie

Department of Mechanical and Industrial Engineering
University of Illinois at Urbana-Champaign
Urbana, IL 61801

Third International Conference on Biaxial/Multiaxial Fatigue, April 3-6, 1989, Stuttgart, FRG

ABSTRACT

The deformation mechanisms of metals under complex nonproportional cyclic loadings are investigated. A comparison of the dislocation substructures in aluminum, copper, and stainless steel under both in-phase (proportional) and 90° out-of-phase (nonproportional) tension-torsion cycling has been made. The increase in cyclic hardening for materials under nonproportional loading is shown to be dependent on the slip mode of the material. Wavy slip materials exhibit no increase in the cyclic hardening level while wavy/planar and planar slip materials show an increase in the cyclic hardening level during nonproportional cycling. Deformation characteristics observed in stress-strain response of materials under nonproportional loading are also described by a simple model for dislocation substructures.

INTRODUCTION

An increasing number of material dependent deformation characteristics have been observed in the stress-strain response of materials subjected to complex nonproportional loadings [1-4]. Stainless steel and copper were found to exhibit additional hardening when cycled with nonproportional loadings [1,2]. The increased hardening of stainless steel from nonproportional cycling was partially recovered when the applied loading changed back to proportional cycling [3]. An abrupt increase in cyclic stress has also been observed when the loading direction is suddenly changed from one principal stress direction to another; this is called cross hardening [4]. These characteristics are found to be material dependent since materials such as 6061-T6 aluminum alloy do not exhibit this behavior [5].

The deformation characteristics of materials under nonproportional loading have been considered in the development of

cyclic plasticity models [3,6]. For instance, the two-surface plasticity model was generalized to allow the radii of the yield and limit surfaces to be dependent on the loading path [6]. A simplified model considering the additional hardening due to nonproportional cycling has been suggested by Benallel and Marquis [3]. A new factor called the nonproportionality parameter has been introduced to predict the stabilized stress-strain response of materials under complex nonproportional loading histories [3]. Many of these path dependent features have been either ignored or poorly modeled [3,6].

The difficulty in developing mechanical models for nonproportional cyclic plasticity results from a lack of detailed understanding about the complex deformation mechanisms in materials during nonproportional loading. For example, different formulations used for defining the nonproportionality parameter have been developed from a trial-and-error approach. As a result, only a limited number of loading cases have been correctly modeled by these parameters [3,6]. From a mechanical point of view, a large number of variables and constants are required for modeling nonproportional cyclic plasticity. Plasticity models have become so complicated that they cannot be easily implemented in engineering analyses [6].

This paper provides a mechanistic interpretation of the observed material behavior. In this paper, the dislocation substructures of aluminum, copper and stainless steels are examined by transmission electron microscope after they have been cycled with complex nonproportional paths. Based on the dislocation substructure, a possible explanation for the material dependence of the nonproportional cyclic hardening is presented. A model for the change in dislocation substructures during nonproportional cycling is developed and used to explain the macroscopically observed stress-strain behavior of metals.

EXPERIMENTAL PROCEDURES

Hot-extruded 1100 aluminum, OFHC copper, and type 310 and 304 stainless steel bars were machined into tubular specimens. A detailed description for the specimen and testing is given in Ref.7. Before testing, elongated grains parallel to the longitudinal axis of the specimen were found in aluminum. Copper and stainless steel exhibited 0.56 mm and 0.013 mm equiaxed grains.

Fig.1(a) to 1(c) show the dislocation substructures of these materials before testing. A high density of dislocations was observed in these materials. Cells with uncondensed walls were also found in aluminum and copper.

Strain-controlled torsion (proportional) and 90° out-of-phase tension-torsion (nonproportional) tests were conducted at room temperature. The tensile strain amplitude ranged from 7×10^{-4} to 3.5×10^{-3} mm/mm. The shear strain amplitude ranged from 9×10^{-4} to 6.1×10^{-3} mm/mm. A list of stabilized stress amplitudes, plastic strain amplitudes, and fatigue lives of these tests are given in Refs.8 and 9. After fatigue testing, small samples were cut from the bulk region of these specimens by diamond blade saw. These samples were mechanically polished into 0.2 mm thickness and jet-electropolished to produce areas for Transmission Electron Microscopy. A Phillips EM400T electron microscope operating at 120kV was used to examine the dislocation substructure. Table 1 is a summary of the dislocation substructure observed in these materials.

DISLOCATION SUBSTRUCTURES

Aluminum

Cell structures were observed in aluminum under both torsion and 90° out-of-phase tension-torsion, Figs.2(a) and 2(b). For the strain range studied, no difference was found in the size of cells. Since aluminum is a wavy-slip material, cross slip can easily occur because of the interaction between dislocations and the constraint of the grain boundaries. As a result, multi-slip structures such as cells are formed in torsionally cycled aluminum even though the maximum shear plane remains fixed. Although a nonproportional loading such as 90° out-of-phase tension-torsion can activate many slip systems by rotating the maximum shear plane during each cycle, the number of slip systems activated by 90° out-of-phase tension-torsion is about the same as torsion. The dislocation substructure resulting from nonproportional loading has been observed to be the same as that for proportional loading.

Copper

Copper has been found to exhibit matrix veins, ladders, walls, cells, and labyrinths upon tension cycling [10,11]. The dislocation substructure of copper under torsion is the same as

that under tension because both are proportional loadings. Structures like matrix veins, ladders, Fig.3(a), walls, and cells, Fig.3(b), were observed in torsionally cycled copper. However, only walls and cells, Fig.3(c), were observed in copper under 90° out-of-phase tension-torsion. A large number of walls that contain features of labyrinths were also noticed, Fig.3(d). The change in the dislocation substructures in copper is related to the wavy/planar slip occurring in copper. In general, the dislocation substructure of polycrystalline copper under proportional loading is a function of the strain amplitude. Since the amount of cross slip is small when copper is cycled by proportional loading with small strain amplitudes, the dislocation substructure is basically single-slip structure, i.e. matrix veins. When the strain amplitude increases, the amount of secondary slip also increases and the dislocation structure changes to ladders, walls, cells, and labyrinths. Under 90° out-of-phase tension-torsion, many slip systems are activated by the rotation of the maximum shear plane. The amount of multi-slip structures in copper under nonproportional loading is larger than that under proportional loading. The minimum strain amplitude for forming multi-slip structures is also decreased [8].

Stainless Steels

Planar dislocations, Fig.4(a), are the major substructure in stainless steels under torsion cycling. As the applied loading changes to 90° out-of-phase tension-torsion, walls, Fig.4(b), cells, Fig.4(c), and labyrinths, Fig.4(d), were observed. The observed differences in dislocation substructures result from the planar slip mode of stainless steel. Under a proportional loading such as torsion, only those slip systems which are close to the maximum shear plane of the applied loading are activated. The resultant substructure consists of single-slip structures such as planar dislocations. Many slip systems are activated during nonproportional loading. The dislocation substructure of stainless steel under 90° out-of-phase tension-torsion becomes multi-slip structures like walls, cells and labyrinths.

THE INCREASED HARDENING BY NONPROPORTIONAL CYCLING

The cyclic stress-strain relations for the materials tested

in this study are plotted in Fig.5 to 7. A major difference is noticed in the nonproportional cyclic hardening of these materials. As shown in Fig.5, aluminum exhibits the same amount of cyclic hardening for both torsion and 90° out-of-phase tension-torsion. Copper and stainless steels show a 30 and 50 percent increase in the stabilized cyclic stress during nonproportional cyclic loading, Figs.6 and 7.

The material dependence of the nonproportional hardening behavior of metals can be explained by the observation of dislocation substructures. Aluminum exhibits the same substructures for both proportional and nonproportional loading. The amount of hardening is not a function of the loading condition. Copper and stainless steels change their dislocation substructures under nonproportional loading and also change their stabilized cyclic stress level. It has been observed that copper single crystals exhibit a 40 percent increase in hardening when the substructure is changed from single-slip to multi-slip structures. Similar mechanisms occur in both copper and stainless steels under nonproportional loading, and an increase in cyclic hardening under nonproportional cycling is expected and observed.

A MODEL FOR NONPROPORTIONAL HARDENING OF METALS

In the last section, observation of dislocation substructures has been used to explain the increased hardening of metals during nonproportional cycling. Nonproportional deformation characteristics such as the recovery of nonproportional hardening and cross hardening have not been addressed in plasticity models. In this section, a simplified model is developed to extend the substructural observations to these problems. With this model, a link between microscopic dislocation substructure and macroscopic plasticity modeling is established.

Two features of the dislocation substructure are important in determining the mechanical properties of materials: the size and anisotropy of the dislocation-free zone. In order to describe these two features, an ellipse defined by area, major/minor axis ratio and major axis direction is suggested to describe the strength and anisotropy of the material.

In general, single-slip structures such as planar dislo-

cations and matrix veins contain a major slip direction. The stress required for dislocation slip is dependent on the straining direction. Anisotropic properties can be expected because a higher stress is required for active dislocations to cross the inactive dislocation wall than that required to move dislocations along the wall. In contrast, the dislocation-free zone in a multi-slip structure such as a cell structure is equiaxed and the mechanical properties are isotropic. Macroscopic properties of the material with multi-slip structures are independent of the loading direction.

In defining the mechanical properties of the material, it has been assumed that the stress required for dislocations to slip is a function of the geometry of the dislocation-free zone. This is indeed the case for metals under cyclic loading. It has been shown by Laird [12], and Kayali and Plumtree [13] that the cyclic stress is inversely related to the dislocation cell size. This observation suggests that under nonproportional loading the limit stress of the material, i.e. the stress at which the stress-strain curve approaches constant stress, can be described by the geometry of the substructures and modeled as an ellipse. The material strength in one direction can be obtained as follows:

$$S(\theta) = \frac{S^*}{r(\theta)^m} \qquad (1)$$

where $S(\theta)$ is the limit stress, $r(\theta)$ is the radius of the ellipse along the straining direction θ, and S^* and m are material constants. Through Eq.(1), a quantitative relation between the dislocation substructure and the mechanical property of materials is defined.

The change of dislocation substructures during nonproportional cyclic loading is modeled by changing the three ellipse variables: the ellipse area (strength), the major/minor axis ratio and the major axis direction (anisotropy). An annealed material has a relatively equiaxed substructure and modeled with a large ellipse area with a major/minor axis ratio equal to one because there is no anisotropy. During cyclic deformation, the size of dislocation-free zone and the ellipse area gradually decreases and approaches a constant value. The anisotropy and the major/minor axis ratio are dependent on the slip mode of the

material. For a wavy-slip material such as aluminum, the major/minor axis is always one since equiaxed dislocation substructures are formed. The deformation substructure of aluminum under either proportional or nonproportional loading is modeled as a circle with decreasing area, Fig.8. For stainless steel, however, the major/minor axis ratio is a function of the loading condition. If the applied loading is proportional, the major/minor axis ratio increases and the deformation state of stainless steel is modeled as an ellipse with a smaller area, Fig.9. The major axis of the ellipse is along the direction of the straining direction. If the applied loading is nonproportional, such as the 90° out-of-phase tension-torsion, the deformation state of stainless steel is the same as that of aluminum and the major/minor axis ratio remains unchanged in the model.

Two more cases are given below to illustrate the change of material substructures under complex nonproportional cyclic loading.

Case I: Stainless Steel under a Sudden Change in Loading Direction

As mentioned earlier, it has been observed that cyclically stabilized stainless steel exhibits a sudden increase in cyclic stress when the loading direction is changed, see Figs.10(a) and 10(b). A schematic diagram showing the possible changes of dislocation substructures during this process is given in Fig.10(c). After many proportional loading cycles, single-slip structures consisting of mainly planar dislocations are formed in the stainless steel, point 1 in Figs.10(b) and 10(c). When the loading direction is suddenly changed, dislocations are forced to slip along the new direction. With increasing cycles along the new direction, both single-slip structures suitable for slip along the new direction and multi-slip structures consisting of smaller dislocation-free zones are formed, points 2 and 3 in Fig.10(c). The cyclic stress increases suddenly because the dimension of the dislocation-free zone along the new straining direction is smaller than that along the previous direction at the initial stage, point 1 in Fig.10(b). This change of dislocation substructures is modeled as an ellipse with the area, major/minor axis ratio and major axis direction being changed appropriately. From point 1 to point 2, the

ellipse has the major axis along the previous straining direction and the value of the major/minor axis ratio is decreased. From point 2 to point 3, the major axis direction changes to the new direction while the major/minor axis ratio increases. The ellipse area is continuously decreased through the whole process. Combined with Eq.(1), the observed cyclic hardening behavior can be described by the change in ellipse model.

Case II: Stainless Steel under a Smooth Change in Staining Direction

Unlike the previous case, the cyclic stress was found to increase smoothly when the straining direction is slowly changed among each cycle, Figs.11(a) and 11(b). For this case, a relatively small angle is maintained between the loading direction and the major axis direction of the ellipse. The deformation state of the material is modeled as a rotating ellipse with decreasing area. Since the observed change in cyclic stress only results from the decrease of ellipse area, the hardening level increases smoothly. Fig.11(c) shows the possible changes of dislocation substructures under this loading condition.

The examples shown above indicate that the ellipse model for dislocation substructures can be used to explain macroscopic material behavior. However, it should also be noted that the observations of dislocation substructures which have been used to support the ellipse model are very generalized and the suggested changes in dislocation substructures is speculative. Further study is necessary to understand the detailed behavior of dislocations upon nonproportional cyclic loading. The suggested model provides a simple way of both explaining the changes in material substructures and describing the macroscopic behavior of materials under complex nonproportional loading. A detailed description for the mathematical formulation of the suggested model and its relation to the plasticity model is presented in Ref.14.

CONCLUSION

The material dependence of nonproportional hardening behavior results from the difference in dislocation slip modes. Wavy-slip materials exhibit the same degree of hardening under both proportional and nonproportional loading. Planar or

wavy/planar slip materials increase their hardening during non-proportional loading as a result of the change in dislocation substructures. Substructural changes are modeled as an ellipse defined by area, major/minor axis ratio and major axis direction. Deformation characteristics of materials under complex nonproportional cyclic loadings have been described.

ACKNOWLEDGEMENTS

This work is supported by the U.S. Department of Energy under Contract DE-AC 02-76ER 01198. The electron microscope work was carried out in the MRL Center for Microanalysis of Materials, University of Illinois, which is supported by the U.S. Department of Energy under Contract DE-AC 02-76ER 01198.

REFERENCES

1. Krempl, E. and Lu, H., "The Hardening and Rate Dependent Behavior of Fully Annealed AISI Type 304 Stainless Steel Under Biaxial In-Phase and Out-Of-Phase Strain Cycling at Room Temperature," ASME Journal of Engineering Materials and Technology, Vol.106, 1984, pp. 376-382.

2. Lamba, H. S. and Sidebottom, O. M., "Cyclic Plasticity for Nonproportional Paths: Part I - Cyclic Hardening, Erasure of Memory and Subsequent Strain Hardening Experiments," ASME Journal of Engineering Materials and Technology, Vol.100, 1978, pp. 96-103.

3. Benallel, A. and Marquis, D., "Constitutive Equations Describing Nonproportional Effects in Cyclic Plasticity," Proceedings of 7th International Conference on Constitutive Laws: Application and Short Course, Tucson, Arizona, 1987

4. McDowell, D. L., Transient Nonproportional Cyclic Plasticity, Ph.D. Thesis, Design and Material Division, Report No.107, Department of Mechanical and Industrial Engineering, University of Illinois at Urbana-Champaign, 1983

5. Krempl, E. and Lu, H., "Comparison of the Stress Responses of An Aluminum Alloy Tube to Proportional and Alternate Axial and Shear Strain Paths at Room Temperature," Mechanics of Materials, Vol.2, 1983, pp. 183-192.

6. McDowell, D. L., "A Two Surface Model for Transient Nonproportional Cyclic Plasticity: Part I and II," ASME Journal of Applied Mechanics, Vol.52, 1985, pp. 298-308.

7. Socie, D. F., Waill, L. A., and Dittmer, D. F., "Biaxial Fatigue of Inconel 718 Including Mean Stress Effects," Multiaxial Fatigue, ASTM STP 853, K. J. Miller and M. W. Brown Eds., ASTM, Philadelphia, 1985, pp. 463-481.

8. Doong, S. H., Socie, D. L. and Robertson, I. M., "Dislocation Substructures and Nonproportional Hardening," Submitted to ASME Journal of Engineering Materials and Technology for Publication.

9. Bannantine, J. A., and Socie, D. F., "Observations of Cracking Behavior in Tension and Torsion Low Cycle Fatigue," Low Cycle Fatigue, ASTM STP 942, H. D. Solomon, G. R. Halford, L. R. Kaisand, and B. N. Leis, Eds., American Society for Testing and Materials, Philadelphia, 1988, pp.899-921.

10. Winter, A. T., Pedersen, O. B., and Rasmussen, K. V., "Dislocation Microstructures in Fatigued Copper Polycrystals," Acta Metallurgica, Vol.29, 1981, pp.735-748.

11. Figueroa, J. C., Bhat, S. P., De la Veaux, R., Murzenski, S., and Laird, C., "The Cyclic Stress-Strain Response of Copper at Low Strains - I. Constant Amplitude Testing," Acta Metallurgica, Vol.29, 1981, pp.1667-1678.

12. Laird, C., "Mechanisms and Theories of Fatigue,"Fatigue and Microstructure, ASM Material Science Seminar, St. Louis, MO., 1978, pp. 149-203.

13. Kayali, E. S. and Plumtree, A., "Stress-Substructure Relationships in Cyclically and Monotonically Deformed Wavy Slip Mode Metals," Metallurgical Transactions A, Vol.13A, 1982, pp. 1033-1040.

14. Doong, S. H., Socie, D. F., Robertson, I. M., "A Nonproportional Cyclic Hardening Model Based on the Dislocation Substructure of Metals," Submitted to ASME Journal of Engineering Materials and Technology for Publication.

Table 1 A Summary of the Dislocation Substructure Observed in Aluminum, Copper, and Type 304 and 310 Stainless Steels, (T = Torsion, I = In-Phase Tension-Torsion, O = 90° Out-of-Phase Tension-Torsion) [8].

MATERIAL	SPEC. I.D.	PATH	MATRIX & VEIN	PLANAR DISLO.	LADDER	DISLO. TANGLE	UNCON-DENCED CELL	WALL	CELL	LABY-RINTH
1100	A109	T							X	
Al	A106	0							X	
	A104	0							X	
OFHC	C001	T	X		X			X	X	
Cu	C005	0					X	X		
	C002	0						X	X	X
304	SS12	I		X				X		
Stainless	SS28	0				X		X		
Steel	SS10	0						X	X	X
310	S105	T		X				X		
Stainless	S101	0				X		X		
Steel	S102	0						X	X	X

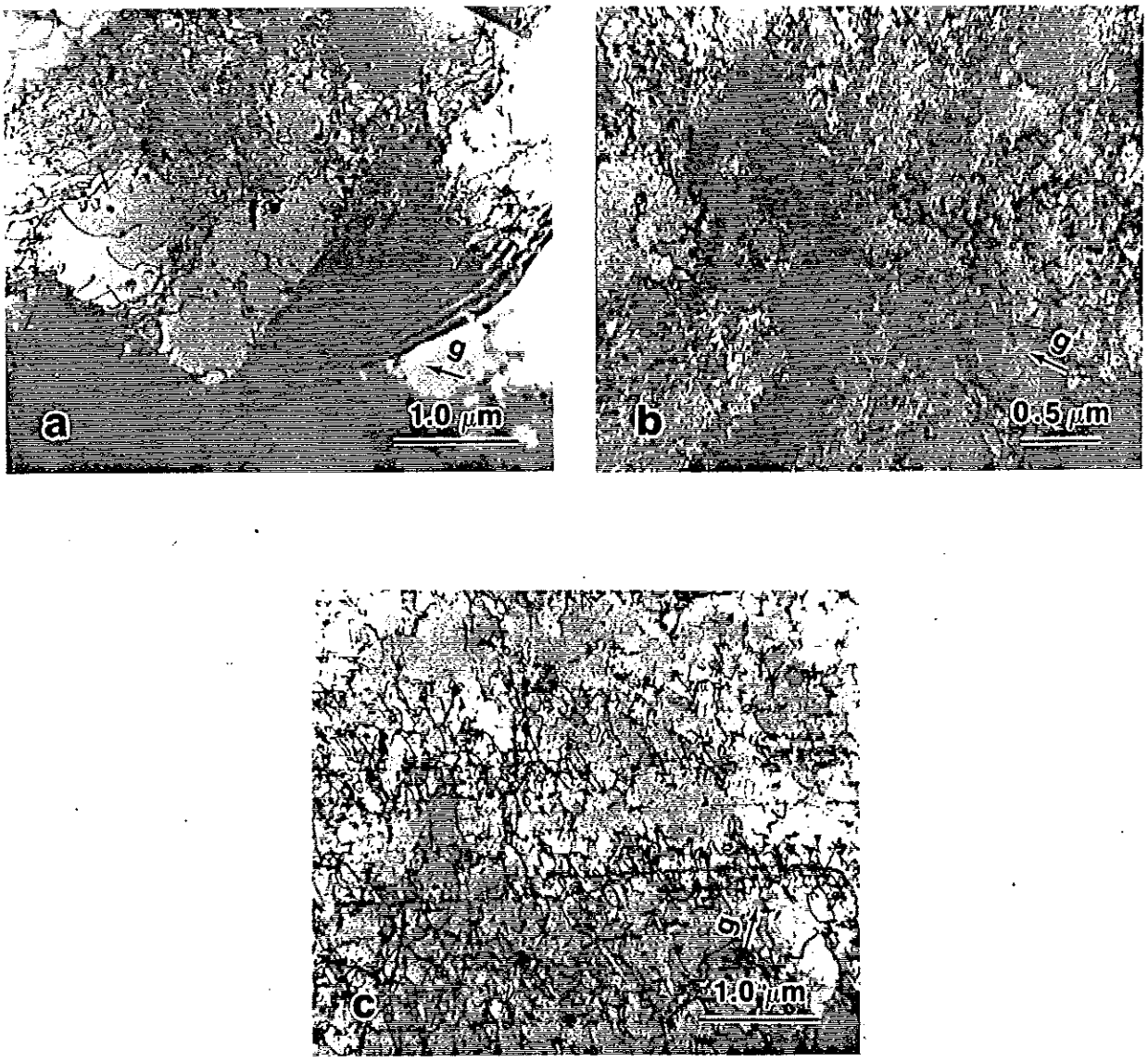

Figure 1 Bright Field Electron Micrographs of the Dislocation Substructures in (a) Aluminum, B = [310], g = [002]; (b) Copper, B = [$\bar{1}$10], g = [$\bar{1}\bar{1}\bar{1}$]; (c) 310 Stainless Steel, B = [211], g = [$\bar{1}$11], Before Fatigue Cycling.

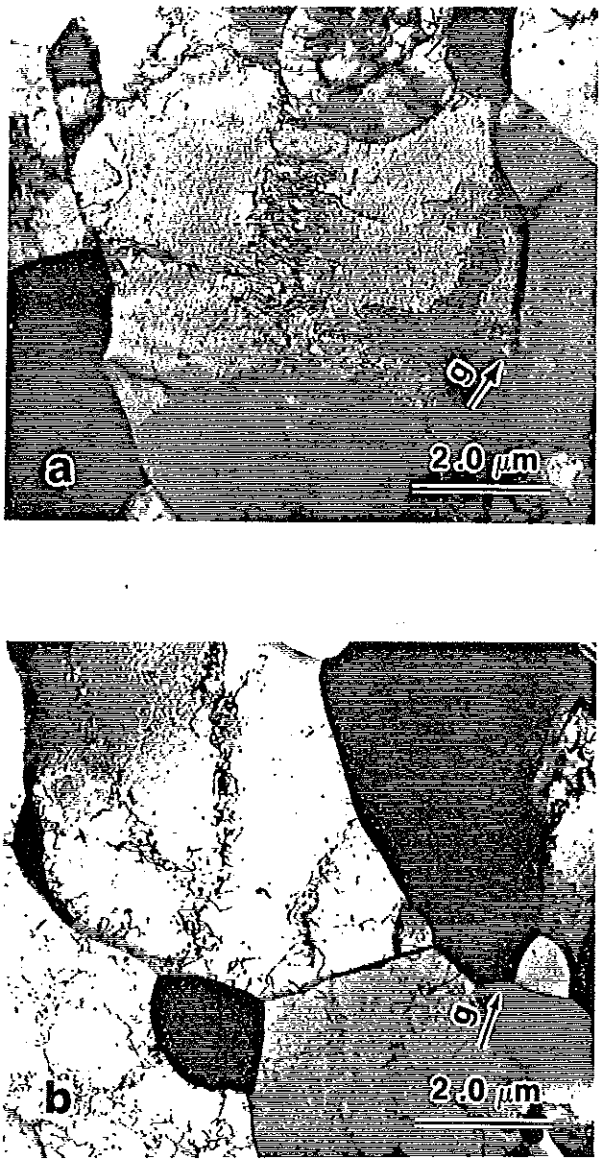

Figure 2 Bright Field Electron Micrographs of the Dislocation Substructures in Aluminum Under (a) Torsion at $\Delta\gamma/2 = 0.0017$, $B = [321]$, $g = [\bar{1}11]$; (b) 90° Out-of-Phase Tension-Torsion at $\Delta\gamma/2 = 0.0025$, $\Delta\xi/2 = 0.0015$, $B = [211]$, $g = [\bar{1}11]$.

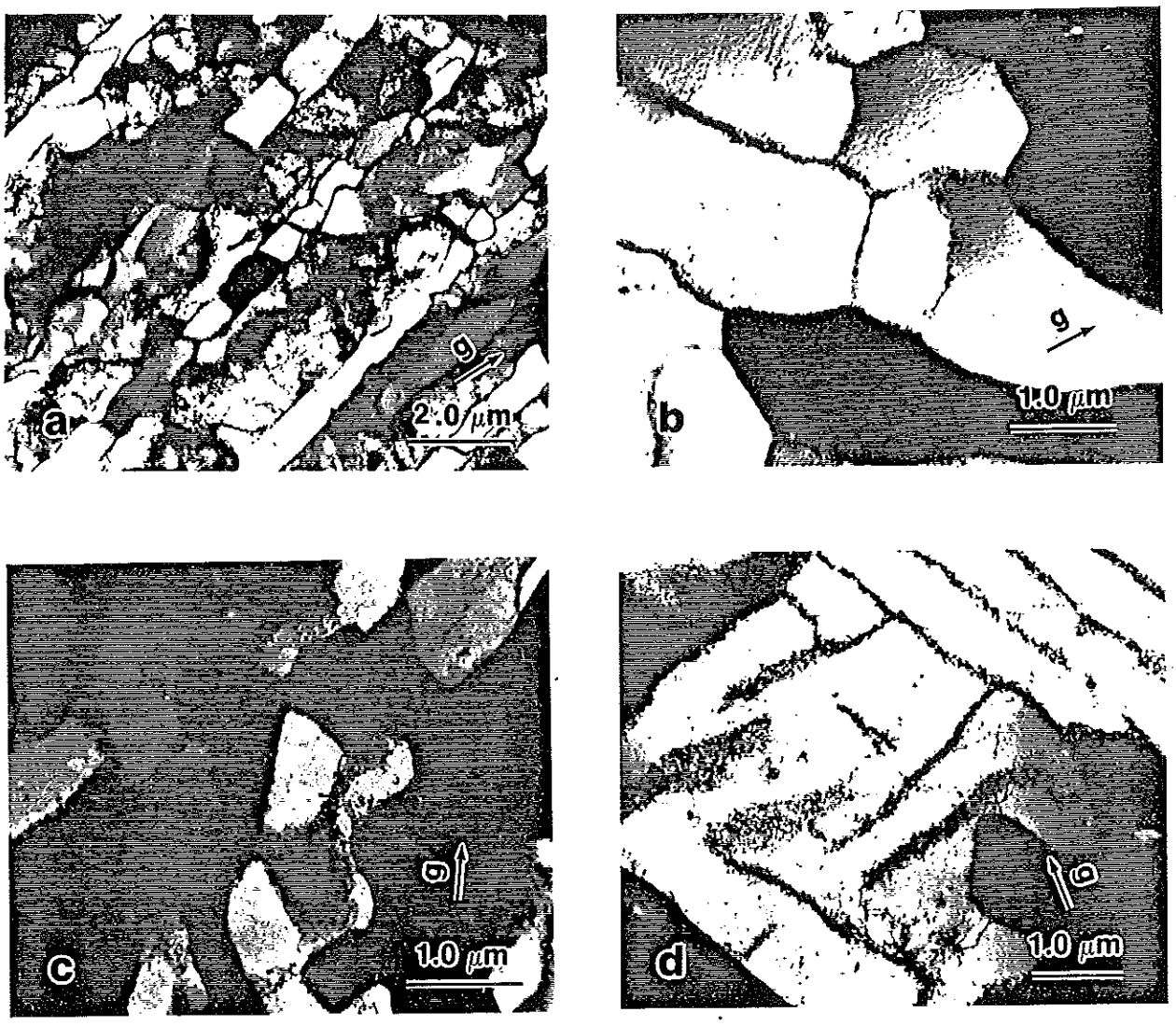

Figure 3 Bright Field Electron Micrographs of the Dislocation Substructures in Copper Under (a) Torsion at $\Delta\gamma/2 = 0.002$, $B = [321]$, $g = [1\bar{1}\bar{1}]$; (b) Torsion at $\Delta\gamma/2 = 0.002$, $B = [110]$, $g = [002]$; (c) 90° Out-of-Phase Tension-Torsion at $\Delta\gamma/2 = 0.002$, $\Delta\xi/2 = 0.0012$, $B = [310]$, $g = [002]$; and (d) 90° Out-of-Phase Tension-Torsion at $\Delta\gamma/2 = 0.002$, $\Delta\xi/2 = 0.0012$, $B = [100]$, $g = [0\bar{1}0]$.

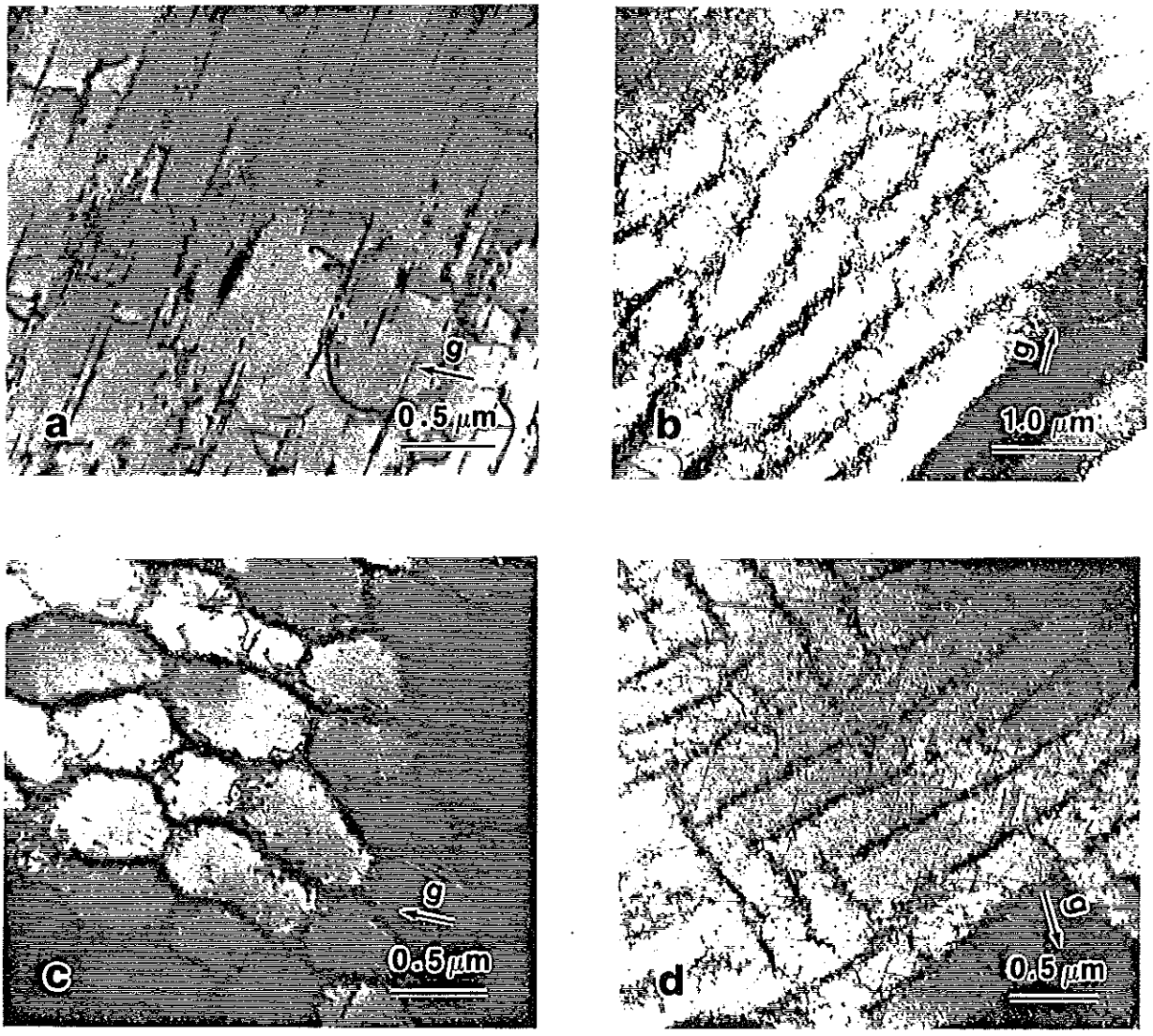

Figure 4 Bright Field Electron Micrographs of the Dislocation Substructures in Stainless Steels Under (a) Torsion at $\Delta\gamma/2$ = 0.0035, B = [110], g = $[1\bar{1}\bar{1}]$; (b) 90° Out-of-Phase Tension-Torsion at $\Delta\gamma/2$ = 0.0061, $\Delta\xi/2$ = 0.0035, B = [110], g = $[1\bar{1}\bar{1}]$; (c) 90° Out-of-Phase Tension-Torsion at $\Delta\gamma/2$ = 0.0061, $\Delta\xi/2$ = 0.0035, B = [210], g = $[00\bar{2}]$; and (d) 90° Out-of-Phase Tension-Torsion at $\Delta\gamma/2$ = 0.0061, $\Delta\xi/2$ = 0.0035,B = [110], g = $[00\bar{2}]$.

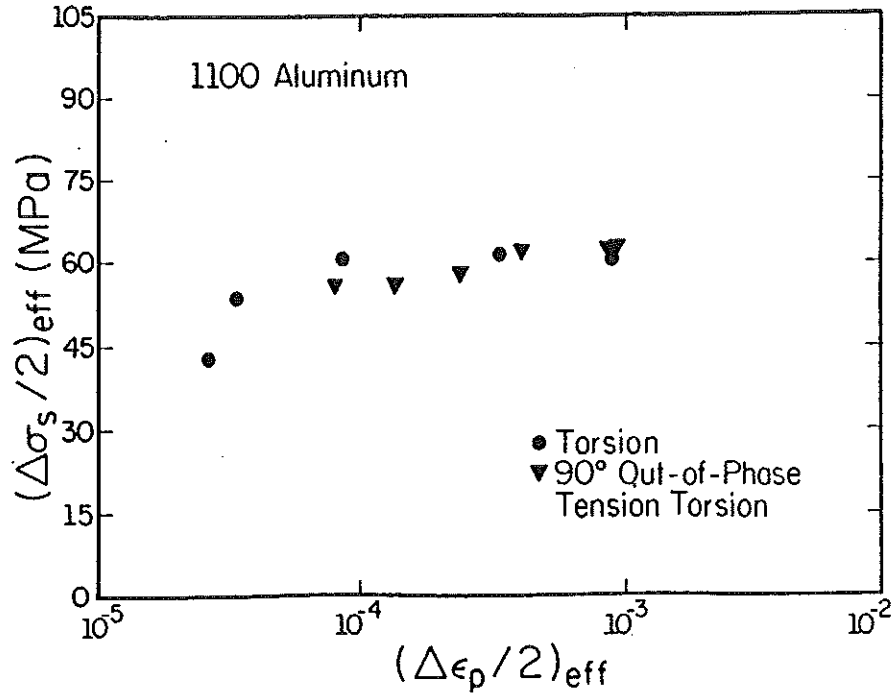

Figure 5 The Stabilized Cyclic Stress of Aluminum as a Function of the Plastic Strain Amplitude [8].

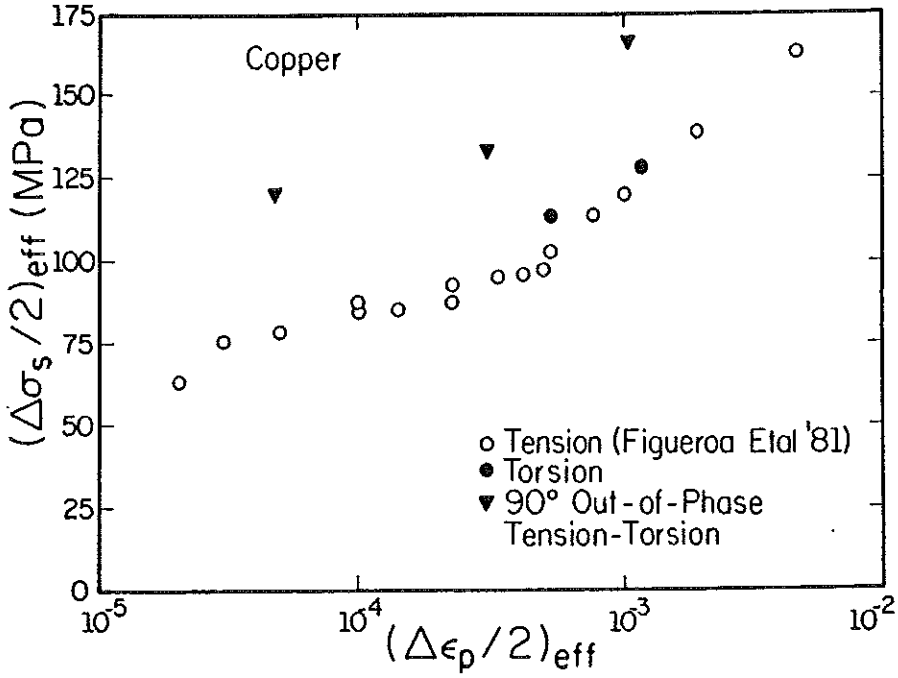

Figure 6 The Stabilized Cyclic Stress of Copper as a Function of the Plastic Strain Amplitude [8].

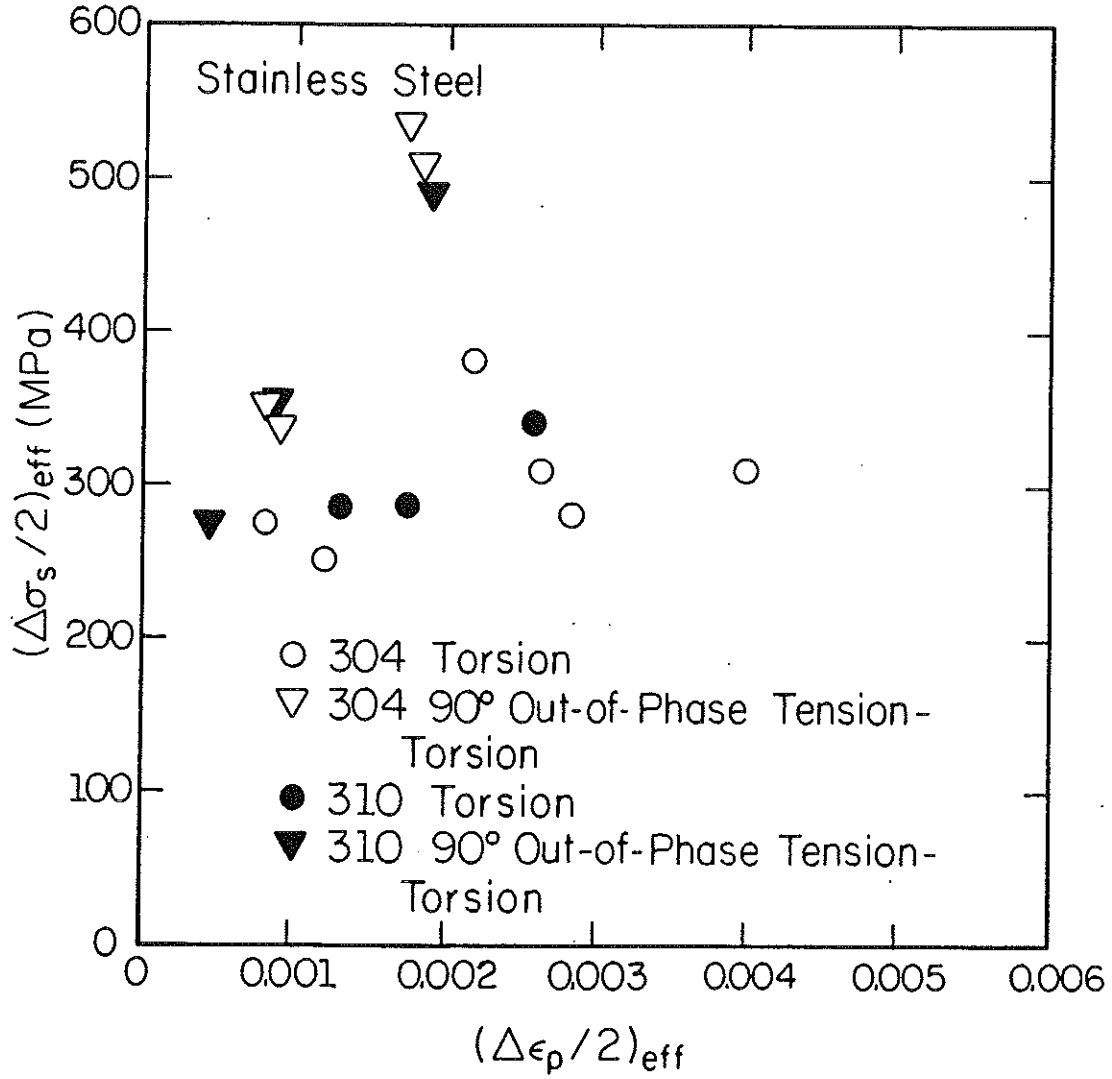

Figure 7 The Stabilized Cyclic Stresses of 310 and 304 Stainless Steels as a Function of the Plastic Stain Amplitude [8].

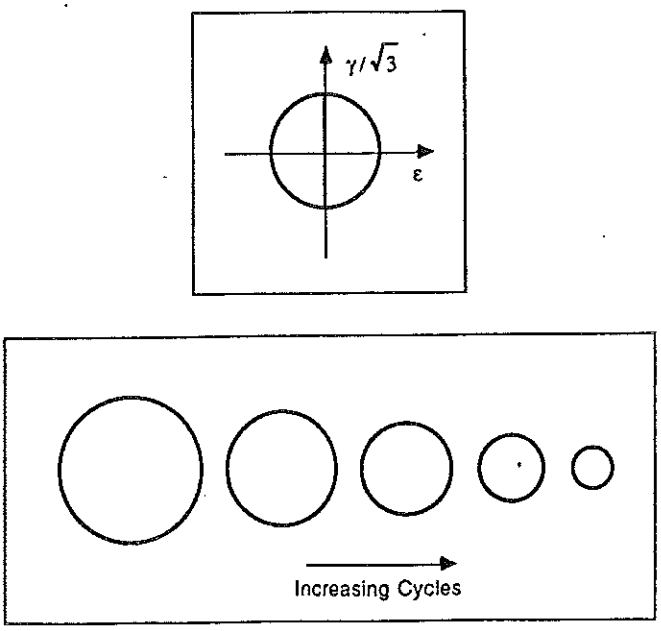

Figure 8 The Deformation State of Aluminum Under Both Torsion and 90° Out-Of-Phase Tension-Torsion [14].

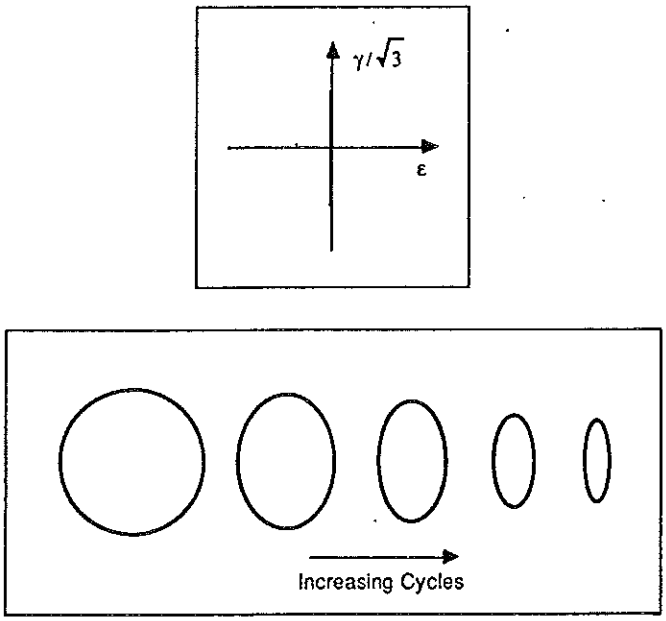

Figure 9 The Deformation State of Stainless Steel Under Torsion [14].

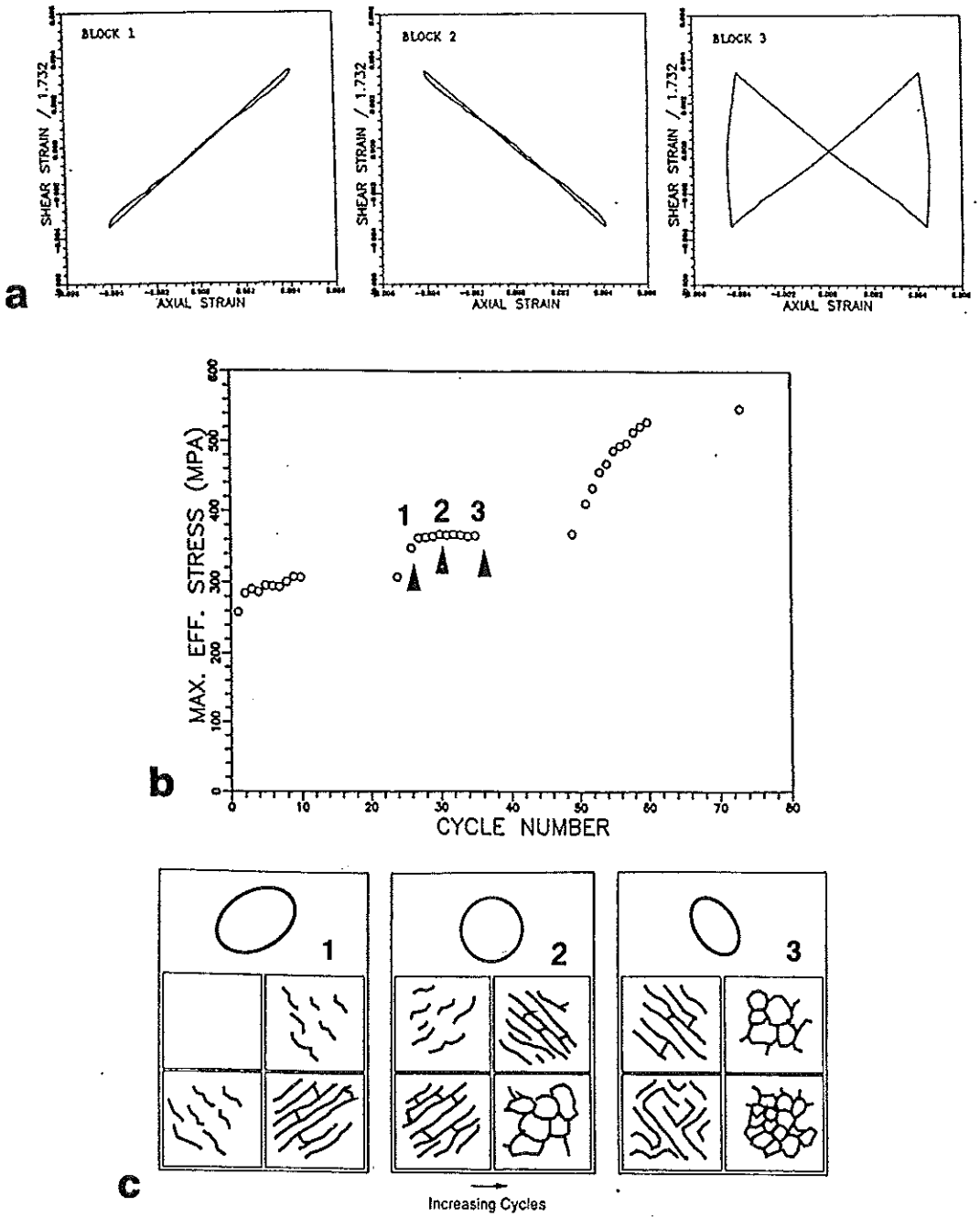

Figure 10 (a) The Deformation State of Stainless Steel Under Loading with a Sudden Change in Straining Direction; Block 1, 25 Cycles; Block 2, 25 Cycles; Block 3, 25 Cycles [4]; (b) The Cyclic Hardening Behavior of Stainless Steel Under the Loading Shown in (a). [4]; (c) Possible Change in the Deformation Substructure of Stainless Steel in the Second Block of the Loading shown in (a) [14].

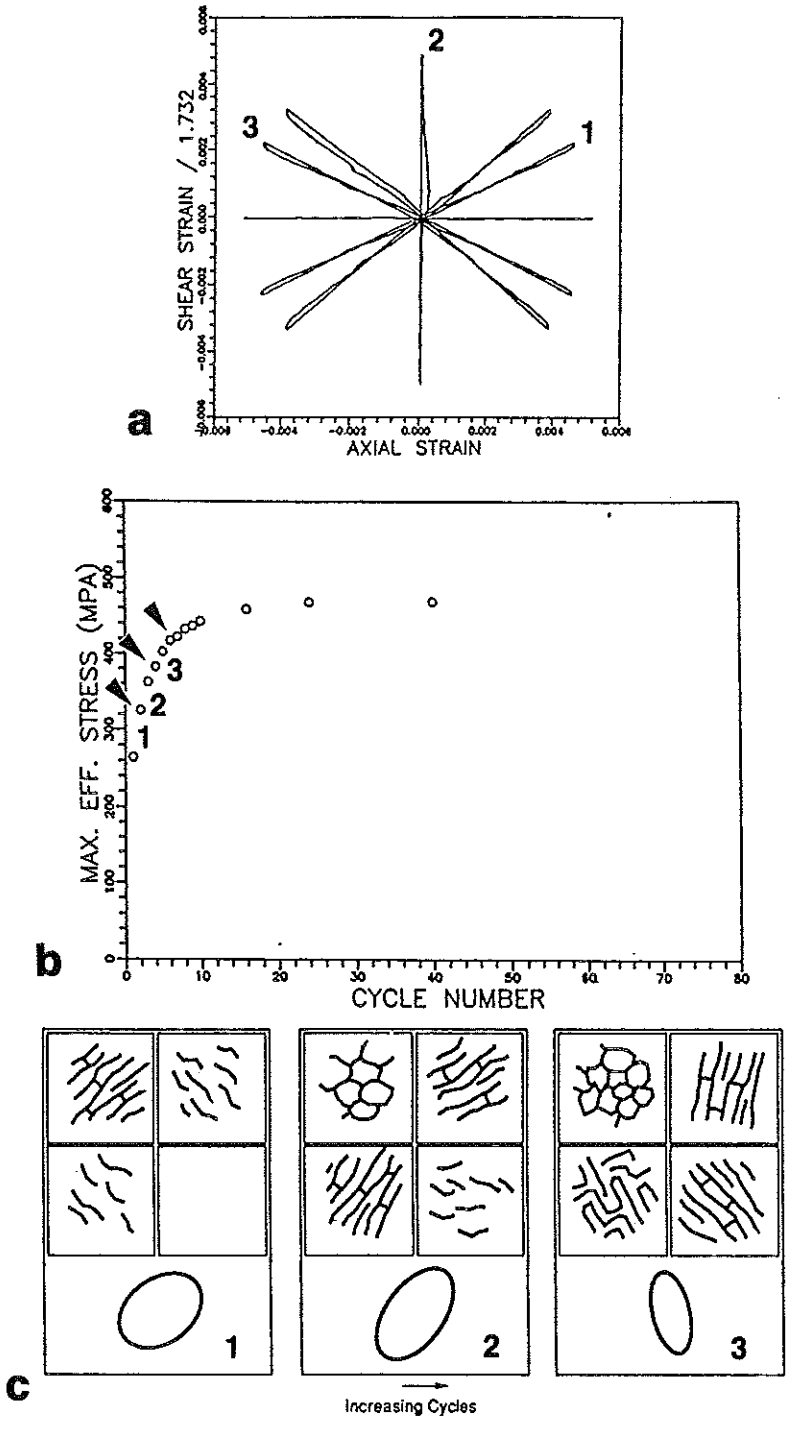

Figure 11 (a) The Deformation State of Stainless Steel Under Loading with a Slow Change in Straining Direction [4]; (b) The Cyclic Hardening Behavior of Stainless Steel Under the Loading Shown in (a) [4]; (c) Possible Change in the Deformation Substructure of Stainless Steel Under the Loading Shown in (a) [14].